Dating of active normal fault scarps in the Büyük Menderes Graben (western Anatolia) and its implications for seismic history

Nasim Mozafari [a, *], Dmitry Tikhomirov [a, b], Ökmen Sumer [c], Çağlar Özkaymak [d], Bora Uzel [c], Serdar Yeşilyurt [a], Susan Ivy-Ochs [e], Christof Vockenhuber [e], Hasan Sözbilir [c], Naki Akçar [a]

[a] Institute of Geology, University of Bern, Bern, Switzerland
[b] Geographical Institute, University of Zurich, Zurich, Switzerland
[c] Department of Geological Engineering, Faculty of Engineering, Dokuz Eylül University, İzmir, Turkey
[d] Department of Geological Engineering, Afyon Kocatepe University, Afyonkarahisar, Turkey
[e] Laboratory for Ion Beam Physics, Swiss Federal Institute of Technology (ETH), Zurich, Switzerland

ARTICLE INFO

ABSTRACT

Fault scarps, if well-preserved, include precise evidence of past earthquakes. Using cosmogenic ^{36}Cl dating, the timing and slip of paleoearthquakes are recoverable beyond the available earthquake archives. One of the appropriate seismically active regions to apply ^{36}Cl dating is western Anatolia, where its deformation is influenced by an N-S extensional regime, where the horst-graben structures are characterized by normal faults.

We have studied well-preserved (meta-) carbonates Kalafat and Yavansu fault scarps in the westernmost part of the Büyük Menderes Graben within western Anatolia. The distribution of cosmogenic ^{36}Cl against height along the fault surfaces indicates that faults experienced minimum three high paleoseismically active phases. The recovered ages of seismic events are ca. 15, 8.4, and 3.6 ka, with vertical components of slip of ca. 0.7, 0.9 and 3.1 m, respectively, for the Kalafat Fault, and ca. 7.9, 3.4, and 2.0 ka with vertical components of slip of ca. 0.6, 3.5, and 2.6 m, respectively, for the Yavansu Fault. The recurrence interval of active periods is generally becoming shortened over time. The ruptures mostly occurred as clustered earthquakes close in time with magnitudes of 6.5—7.1. The vertical slip rates of >0.1, 0.1, and 1.5 mm/yr, and >0.1, 0.8, and 1.9 mm/yr were calculated for the Kalafat and Yavansu faults, respectively. Long-term slip rates were also estimated about 1.0 and 0.6 mm/yr for the Kalafat and Yavansu faults, respectively. Considering the fault lengths, they are capable of producing earthquakes with magnitudes larger than 6.5, and are seismogenic faults.

1. Introduction

The Western Anatolian Extensional Province is one of the most seismically active regions in the world, where large-scale horst-graben structures control its tectonic behavior (e.g., Dewey and Şengör, 1979). This is mainly due to the Africa-Eurasia collision along the Hellenic-Cryprian Arc, and an approximately N-S extensional regime as its back arc area (e.g., Dewey and Şengör, 1979; Barka and Reilinger, 1997; Koçyiğit and Özaçar, 2003). The graben systems are characterized by normal faults occasionally occurring in carbonates (Fig. 1), which are ideal to apply exposure dating using cosmogenic ^{36}Cl. Reconstruction of paleoearthquakes in terms of their timing and magnitude is crucial to estimate the timing and magnitude of probable future earthquakes (e.g., McCalpin, 2009). The occurrence of many destructive historical and instrumental earthquakes in the active region of western Anatolia sheds light on the importance of paleoseismic studies in order to reduce the potential damage following significant earthquakes.

In this study, we focused on the Büyük Menderes Graben, one of the main graben systems of western Anatolia, where many active faults potentially threaten thousands of lives (Fig. 2). The adjacent Kalafat and Yavansu faults are two such faults in the southeast of Kuşadası. There is no historical or instrumental earthquake directly

Fig. 1. Simplified geological map of western Anatolia (modified after Akçar et al., 2012; Sümer et al., 2013, Mozafari et al., 2019). The yellow stars show the locations of the sampling sites of this study in Kalafat and Yavansu faults along with Priene-Sazlı Fault (Mozafari et al., 2019), Mugırtepe Fault (Akçar et al., 2012) and Manastır Fault (Tikhomirov, 2014). The black box gives location of Fig. 2. (For interpretation of the references to color in this figure legend, the reader is referred to the Web version of this article.)

attributed to these two faults. However, the oldest known historical earthquake closest to the two faults is dated back to 1751 AD (e.g., Soysal et al., 1981). There were also instrumental earthquakes in the surrounding area, among which the most destructive one occurred in 1955, and is related to Priene-Sazlı Fault (Altunel, 1988). However, in order to evaluate the seismic pattern of earthquakes on any particular fault, more seismic data over a wider time span is needed. We modeled the time-slip history of the Kalafat and Yavansu faults over a large time-scale (Figs. 1 and 2). Our goals were to reconstruct the age and vertical components of slip of past earthquakes, calculate the slip rates through time and estimate the magnitude of future earthquakes. To accomplish this, a total 122

samples were collected from both fault scarp surfaces for cosmogenic ^{36}Cl analysis. Our results show the occurrence of at least three major periods of seismic events characterized by clustered earthquakes occurred close in time from 6.4 to 7.1 in magnitude on both faults since Late Pleistocene.

2. Study area

Büyük Menderes Graben is one of the main horst-graben systems in western Anatolia. This crustal-scale tectonic structure extends approximately 140 km between the Denizli Basin in the east with an E-W trend and continues with a change in strike to a NE-
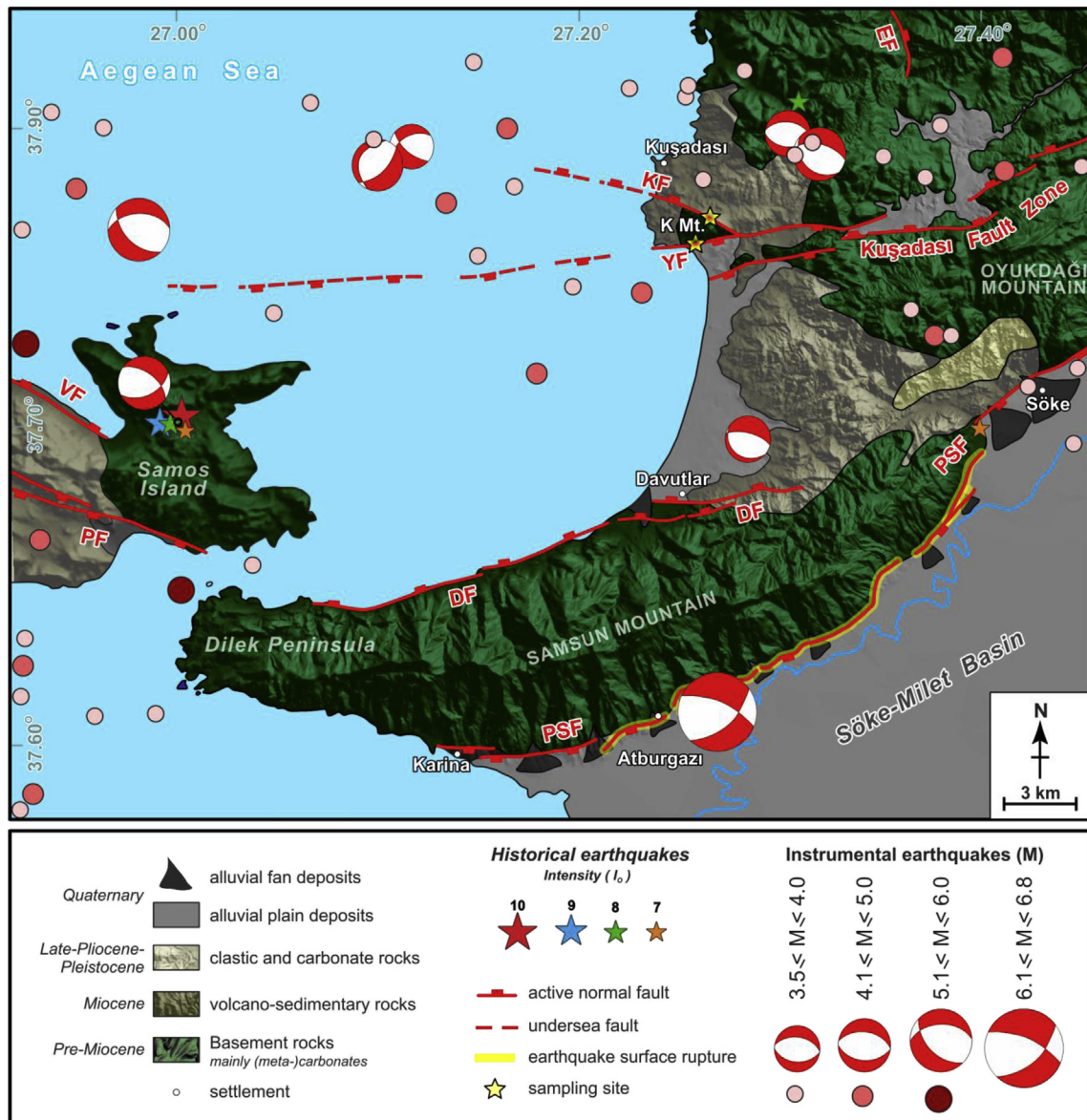
Fig. 2. Geological map of Kuşadası area, including location of historical and instrumental earthquakes (modified after Hancock and Barka, 1987; Sümer et al., 2012; Emre et al., 2016). YF: Yavansu Fault, KF: Kalafat Fault, PSF: Priene-Sazlı fault, DF: Davutlar Fault, K Mt.: Kalafat Mountain.

SW trend towards the Aegean Sea in the west (Fig. 1). The horst-graben structure of the graben is strongly dominated by normal faults in varying scales (Gürer et al., 2009; Sümer et al., 2013; Emre et al., 2016). The Priene-Sazlı Fault, Davutlar Fault and the Kuşadası Fault Zone including several north- and south-facing normal fault segments constitute the westernmost part of the graben (Fig. 2). Kuşadası Fault Zone intersects the Oyukdağı Mountain with a general trend of ENE-WSW, and splays into two branches named the Kalafat and Yavansu Faults, as the north- and south-facing fault scarps, respectively.

The Kalafat Fault is generally a WNW-trending and N-dipping normal fault with a minor dextral component, which delimits the northern side of the Kalafat Mountain (Figs. 2 and 3a). The meta-carbonates of Cycladic Massif constitute its footwall, while the hanging wall is made up of volcano-sedimentary rocks of Miocene age, covered by tens of meters of colluvium in front of the fault. The fault length is approximately 15 km with the possible continuation under the Aegean Sea. The Yavansu Fault is basically an E-W-

trending and S-dipping normal fault, located on the southern side of Kalafat Mountain, which juxtaposes Quaternary sediments in the hanging-wall against meta-carbonates of Cycladic Massif in the footwall (Fig. 4a). The fault has length of approximately 10 km based on Duman et al. (2011) and this study. According to Hancock and Barka (1987), the fault length is elongated roughly 25 km on the mainland Turkey and 25 km under the sea towards the Island of Samos (Fig. 2).

The Kuşadası area was seismically active in the time span of 1751–1893 AD (e.g., Soysal et al., 1981). Most of the seismic events occurred in the western segment of the Yavansu Fault that extended to the Island of Samos (Fig. 2). The largest instrumental earthquake close to the study area was the 1955 Söke-Balat earthquake, related to the Priene-Sazlı Fault, whose trend is sub-parallel to the Yavansu Fault (Fig. 2). A comparison of the focal mechanism solution of the 1955 earthquake with the Yavansu Fault structural measurements indicates the similarity of their structural patterns (Hancock and Barka, 1987). The activity of the Yavansu
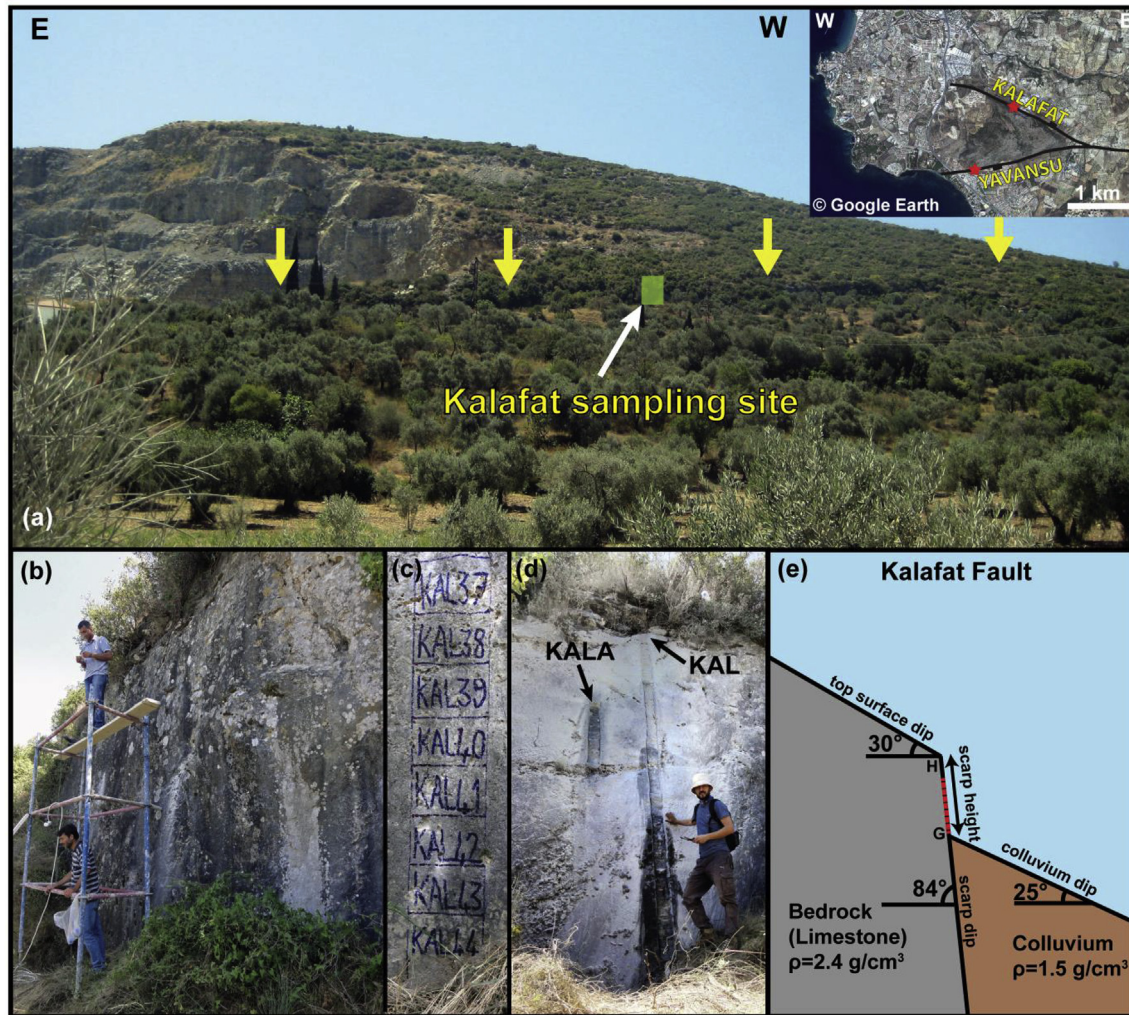
Fig. 3. (a) Field view of the Kalafat Fault and sampling site; The yellow arrows trace the fault exposed surface; (b) Approximately vertical Kalafat Fault surface; (c) Fault scarp surface showing the lowest marked sampling slabs to be cut and collected; (d) KAL and KALA strips after the sample collections; and (e) Schematic sketch of Kalafat Fault showing input parameters of the fault scarp used for modeling, including scarp height, scarp dip, colluvium dip, top surface dip and density of the bedrock and colluvium. Red dashed line shows the sampled surface. (For interpretation of the references to color in this figure legend, the reader is referred to the Web version of this article.)

Fault was proven by several pieces of evidence, which indicate the occurrence of at least one slip during the Quaternary (Hancock and Barka, 1987). These are documented by: (i) brecciated colluvium in the vicinity of the uppermost slip planes; (ii) brecciated colluvium affected by several sub-ordinate slip surfaces; (iii) matrix and clasts occasionally cut by comb-fractures in patches of colluvium; (iv) occasional striations of colluvium material located in corrugations; and (v) locally displaced colluvium layering by small reverse faults, which cut the slip planes of normal dip-slip lineations.

3. Method and sampling

The potential of cosmogenic ^{36}Cl dating method has been proven worldwide on carbonate normal faults during the last 20 years (Zreda and Noller, 1998; Mitchell et al., 2001; Benedetti et al., 2002, 2003; 2013; Palumbo et al., 2004; Carcaillet et al., 2008; Schlagenhauf et al., 2010, 2011; Akçar et al., 2012; Tikhomirov, 2014; Mouslopoulou et al., 2014; Tesson et al., 2016; Cowie et al., 2017; Mechernich et al., 2018; Beck et al., 2018; Mozafari et al., 2019; Tesson and Benedetti, 2019). In this dating method, measured cosmogenic ^{36}Cl concentrations in the outermost couple of centimeters of the fault scarp surface are considered as a function

of scarp height. Cyclic seismic activity of a fault causes a non-linear profile in cosmogenic ^{36}Cl concentrations, which enables determination of the timing of past ruptures and the vertical component of their slips. Based on the magnitude of associated ruptures, the short-term and long-term slip rates can be calculated. Each rupture exposes at the surface a section of the scarp previously covered by colluvium. Consequently, the exposed section accumulates ^{36}Cl at a higher rate during the period of quiescence. As long as a fault section is covered by hanging-wall colluvium sediments, secondary cosmic rays create an exponential pattern of cosmogenic ^{36}Cl reducing with depth. In a successive seismic pattern, each sharp discontinuity in the cosmogenic ^{36}Cl concentration profile indicates an activity period of the fault, whereas the convex intervals of ^{36}Cl profile mark the dormancy periods. The distance between two adjacent inactivity marks is the vertical component of slip (for further information see Mozafari et al., 2019).

Our sampling sites of the Kalafat and Yavansu fault scarps are located on opposite slopes of the Kalafat Mountain, along the Kuşadası Fault Zone (Fig. 2). Appropriate sampling sites were selected following the instructions of Mitchell et al. (2001) and Tikhomirov (2014). We selected the sampling surfaces after full consideration of fault outcrops in different localities along their
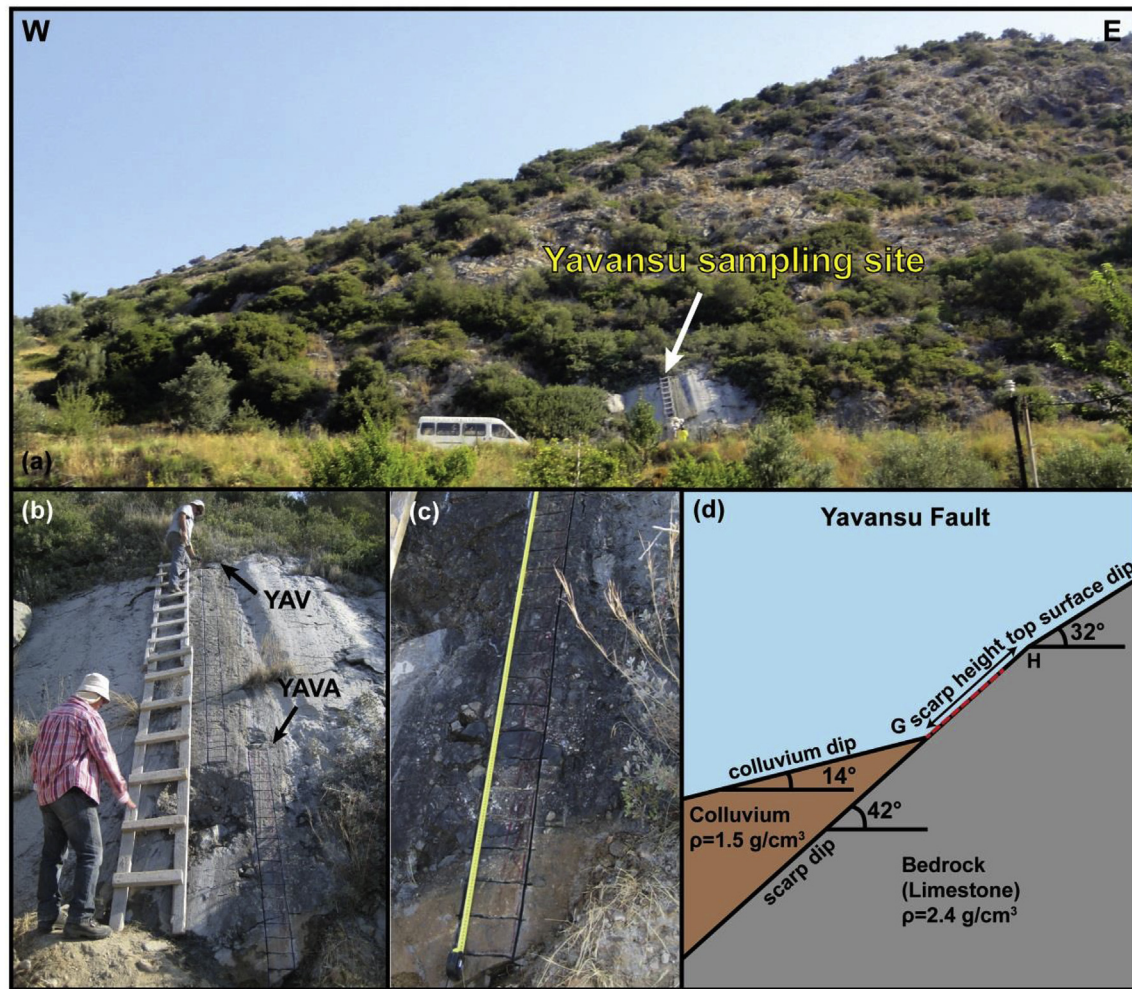
Fig. 4. (a) Field view of the Yavansu Fault and sampling site; (b) YAV and YAVA continuous strips before sample collection; (c) More detailed view of YAVA sampling strip showing the colluvium level; and (d) Schematic sketch of Yavansu Fault showing input parameters of the fault scarp used for modeling, including scarp height, scarp dip, colluvium dip, top surface dip and density of the bedrock and colluvium. Red dashed line shows the sampled surface. (For interpretation of the references to color in this figure legend, the reader is referred to the Web version of this article.)

length with the minimum amount of weathering and erosion. No weathering patterns were observed on the selected surfaces. However, erosion rate uncertainty is considered in modeling. We sampled the well-exposed N82E, 82°−85° NW-dipping Kalafat Fault (Fig. 3a and b). In total, 54 samples each measuring 15 cm wide by 10 cm high were collected with a chisel and hammer. A total of 4.6 m in height of the fault surface was sampled parallel to the slip direction. We did not sample the top 1.6 m of the fault surface due to heavy erosion and weathering. The boundary between the exposed part of the fault scarp and the part covered by colluvium was evidenced by the freshness of the fault surface and determined to be approximately 10 cm above the recent ground level (Fig. 3c). From the Kalafat Fault surface, 45 of the samples were collected along a main strip (KAL), of which one is considered as the sample below the ground level. Nine additional samples were also taken from a parallel strip (KALA) at the same heights corresponding samples on part of the KAL, and with approximately 1 m of horizontal separation (Fig. 3d).

On the other side of the mountain, the N74W, 40°−44° SW-dipping scarp surface in the lowermost part of the Yavansu normal fault escarpment was sampled (Fig. 4a). In total, 68 slabs

were collected from heights of approximately 6.6 m to the ground level, along two strips, YAV and YAVA, parallel to the slip direction (Fig. 4b). The top 60 cm of the fault surface was not sampled, due to weathering and vegetation. Similar to the Kalafat Fault, the colluvium position was determined based on the difference in freshness of the exposed and already covered surface at about 40 cm above the recent ground level (Fig. 4c). Accordingly, four samples were taken below the former ground level. As the modeled concentration profile specifically depends on the geometry of the fault scarp, the scarp dip, scarp height, top surface dip and colluvium dip were measured (Figs. 3e and 4d) (Tikhomirov, 2014). The specific position of each sample along the sampling strips was recorded. Furthermore, the density of the colluvium was measured with a bucket of defined volume and a balance in the field. Water content of bedrock and colluvium were estimated to be 0.2 and 1%, respectively.

4. Cosmogenic ^{36}Cl analysis

All samples were prepared at the Surface Exposure Dating Laboratory of University of Bern, following the protocol of Stone

et al. (1996) and Ivy-Ochs et al. (2004, 2009), and the isotope dilution method (Elmore et al., 1997; Ivy-Ochs et al., 2004). First, the slabs were cut parallel to the surface to a thickness of 2.5–3 cm. After crushing, they were sieved into a 0.25–0.4 mm size fraction. A hand magnet was used to separate any metal-chips from crushing material. The crushed material was leached in 75 ml of 2 M of HNO_3 overnight, and then rinsed four times with ultrapure water (18.2 MΩ cm) to remove non-in situ Cl (Zreda et al., 1991). The same leaching procedure was repeated. The samples were dried on a hotplate at 60 °C. Approximately 12 g of each sample, 1 m apart along the height of the fault scarp, were taken as proxies, and analyzed by ICP and ICP-MS for major and trace elements at Actlabs Analytical Services, Canada. Additionally, the Ca concentration of each sample was also measured.

Samples were prepared in batches of 15 samples, and were accompanied with one full process blank to be processed at once. Samples were spiked with around 2.5 mg of pure ^{35}Cl in order to measure the total Cl concentration (^{35}Cl, ^{37}Cl) (Ivy-Ochs et al., 2004, 2009), and were dissolved with HNO_3. Determination of the Cl concentration is required in order to calculate (1) ^{36}Cl concentration in the sample; (2) ^{36}Cl production rate by low-energy neutron capture on ^{35}Cl; and (3) non-cosmogenic subsurface production of ^{36}Cl. The samples were then centrifuged to remove impurities. In order to precipitate AgCl, 10 ml of $AgNO_3$ was added to the supernatant at 200 °C in the dark. After collection of the precipitated AgCl, dissolution was achieved with 2 ml of NH_4OH. The samples were centrifuged in order to eliminate cations. Afterwards, $BaSO_4$ was precipitated by addition of $Ba(NO_3)_2$ to the supernatant, in order to avoid interference of ^{36}S isobar with ^{36}Cl during Accelerator Mass Spectrometry (AMS) measurements. AgCl was precipitated for the second time. In the final step, the AgCl decant was recovered and rinsed with ultrapure water. AgCl sample pills were pressed into tantalum-lined copper target for AMS measurements.

The measurements of total Cl and ^{36}Cl concentrations were done from a single target at ETH AMS facility following the isotope dilution method (Christl et al., 2013; Synal et al., 1997; Ivy-Ochs et al., 2004). The stable ratio of $^{37}Cl/^{35}Cl$ was normalized to the neutral ratio $^{37}Cl/^{35}Cl = 31.98\%$ of K382/4N standard and the machine blank. Ratios of $^{36}Cl/^{35}Cl$ derived from the measurements were normalized to the ETH internal standard K382/4N with a value of $^{36}Cl/Cl = (17.36 \pm 0.35) \times 10^{-12}$ (Christl et al., 2013). The sulfur correction of the measured $^{36}Cl/^{35}Cl$ ratio was insignificant. Furthermore, measured $^{36}Cl/^{35}Cl$ ratios of the sample were corrected for a procedural blank of $(1 \pm 0.02) \times 10^{-15}$, which was less than 1% for the samples.

5. Results

The position of the samples along the scarp height, the sample thickness, the cosmogenic ^{36}Cl concentration and its uncertainty, the natural chlorine concentration, as well as calcium, oxygen and carbon concentrations of the samples from the Kalafat and Yavansu fault scarps are given in Tables S1 and S2. Major and trace elements were measured in eight and seven proxy samples in the Kalafat and Yavansu fault scarps, respectively, whose average values were used for modeling (Tables S3 and S4). The fault scarp parameters are given in Table S5. The density of the colluvium was measured as 1.5 g/cm^3 in the field and density of the scarp limestone is considered to be 2.4 g/cm^3. Measured cosmogenic ^{36}Cl concentrations with their corresponding 1σ errors were plotted versus height for each strip (Fig. 5a and b). The concentration of cosmogenic ^{36}Cl varies between $(1.049 \pm 0.046) \times 10^5$ at g^{-1} to $(3.111 \pm 0.114) \times 10^5$ at g^{-1} along the Kalafat Fault (Fig. 5a) and between $(0.793 \pm 0.047) \times 10^5$ at g^{-1} to $(2.593 \pm 0.126) \times 10^5$ at g^{-1} along the Yavansu Fault (Fig. 5b).

We analyzed the Kalafat and Yavansu fault data with the FSDT Matlab® code, which denotes -Fault Scarp Dating Tool- (Tikhomirov, 2014). The fault scarp shielding model (provided as supplementary material; after Tikhomirov et al., 2014) was used to calculate the cosmogenic ^{36}Cl accumulation. In order to reconstruct a realistic time-slip history, the Monte-Carlo method was used. The FSDT Matlab® code considers all factors leading to produce ^{36}Cl, which are high energy neutrons, fast and negative muons, as well as thermal and epithermal neutrons (Liu et al., 1994; Phillips et al., 1996, 2001; Stone et al., 1996, 1998; Alfimov and Ivy-Ochs, 2009; Schimmelpfennig et al., 2009). The model considers the given scenario in terms of number of ruptures, timing and associated slips, beginning of exposure and erosion rate. The code applies default rates of ^{36}Cl by high-energy neutron spallation on Ca of 48.8 ± 3.5 at g^{-1} yr^{-1} (Stone et al., 1996), on K of 170 ± 25 at g^{-1} yr^{-1} (Evans et al., 1997), on Ti of 13 ± 3 at g^{-1} yr^1 (Fink et al., 2000), and on Fe of 1.9 ± 0.2 at g^{-1} yr^{-1} (Stone, 2005). It also applies the production rate of epithermal neutrons from fast neutrons in the atmosphere at the land/atmosphere interface of 760 ± 150 n/g^{-1} yr^{-1} (Alfimov and Ivy-Ochs, 2009); while the scaling scheme of Stone (2000) is also used. The model output is displayed as the ^{36}Cl concentrations of the samples versus position along fault scarp in meters, in which each discontinuity defines a distinct period of activity of the fault. The measured data are compared with the modeled data, and a best fit model, which is more consistent with the measured data, is accepted. The number of earthquakes modeled by FSDT is the minimum number, because the program only detects earthquakes with high magnitudes that are capable of displacing the faults (Tikhomirov, 2014). The model uncertainties are subjective to a variety of parameters such as measurement errors of AMS, parent elements, rock density, production rates, and estimation of scarp geometry and can be considered about 25% (2σ) and 15% (2σ) of modeled age and slip, respectively. Consequently, the earthquakes resulting in age and slip within the 2σ uncertainties are detected as apparent continuous slip (after Akçar et al., 2012; Tikhomirov, 2014).

In the first step of modeling using FSDT, different scenarios with different numbers of earthquakes, age and slip as well as erosion rates were tested. Afterwards, the scenarios with the best statistical criteria were focused upon. The best fit solutions for each scenario tested for the faults are summarized in Table S6. The scenarios with three earthquakes show the best statistics with RMSw = 1.7492, $X^2 = 3.6007$ and AICc = 233.9766 for the Kalafat Fault, and with RMSw = 1.1422, $X^2 = 1.4768$ and AICc = 346.8627 for the Yavansu Fault. The scenario of three earthquake events for the Kalafat Fault gave the best fit, with the beginning of exposure at ca. 22 ka. The ages of the three earthquake events are ca. 15.3 ± 3.8 ka, 8.4 ± 2.1 ka, and 3.6 ± 0.9 ka, with vertical components of associated slip of 0.7 ± 0.1 m, 0.9 ± 0.1, and 3.1 ± 0.5 m. (Fig. 6a). The average slip rates from the oldest to youngest reconstructed rupture (EQ3 to EQ1) were estimated to be > 0.1, 0.1 and 1.5 mm/yr (Fig. 7a), while the long-term slip rate was calculated to be 0.6 mm/yr. The fault does not follow a regular recurrence interval with ca. 6.9 and 4.8 kyr difference in the time span between earthquakes.

The scenario of three earthquake events for the Yavansu Fault gave the best fit, with the beginning of exposure at ca. 12 ka. The ages of the three earthquake events are 7.9 ± 2.0 ka, 3.4 ± 0.8 ka, and 2.0 ± 0.5 ka with vertical components of associated slip of 0.6 ± 0.1 m, 3.5 ± 0.5 m, and 2.6 ± 0.4 m, respectively (Fig. 6b). The vertical distances between ruptures give an average value of vertical slip rates greater than 0.1 mm/yr for the oldest earthquake and 0.8 and 1.9 mm/yr for the second and third earthquakes during the seismic activity of the Yavansu Fault (Fig. 7b). The long-term slip rate was calculated to be ca. 1 mm/yr, taking into account that 6.1 m of slip occurred in the time span between the oldest and the
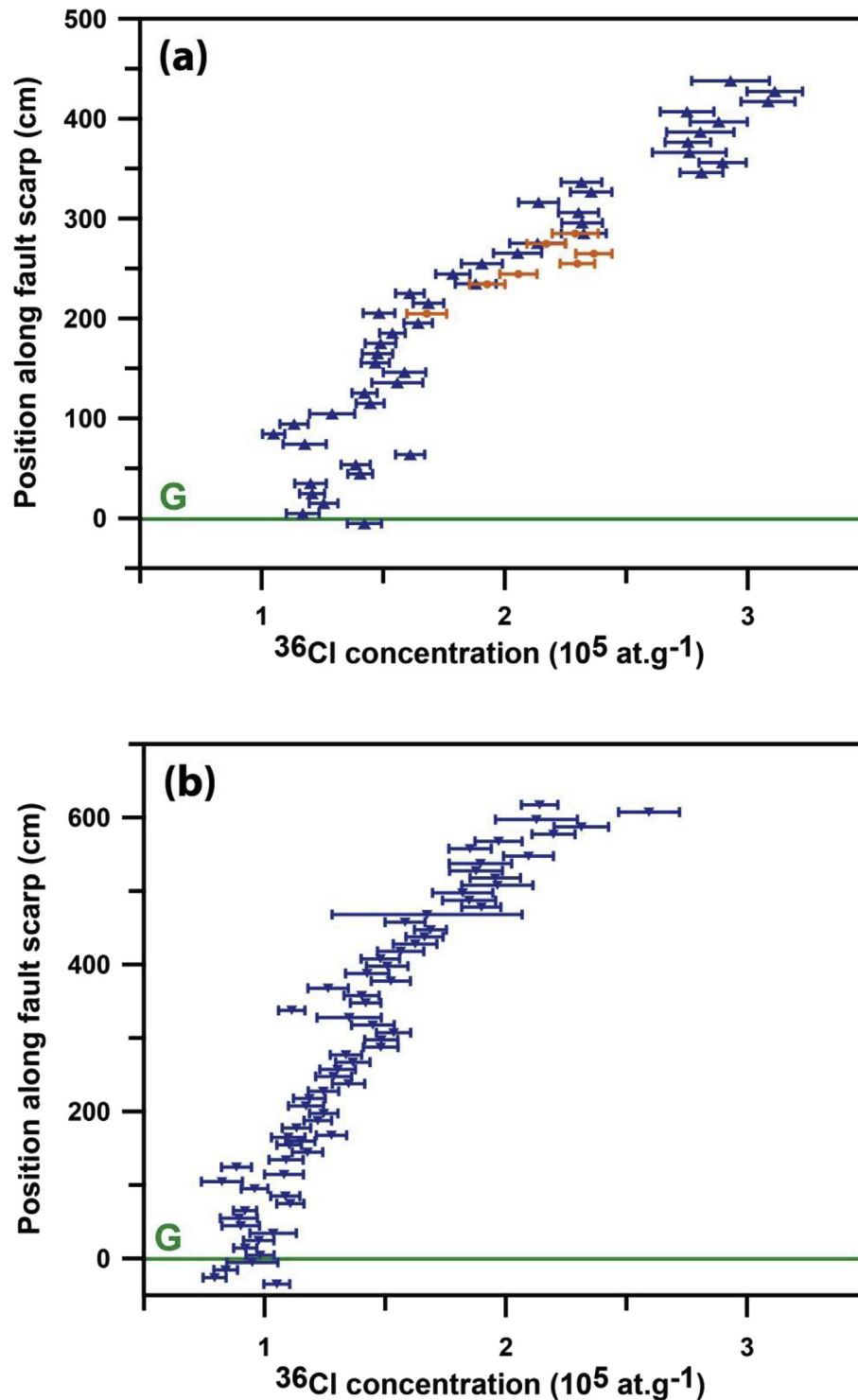
Fig. 5. (a) Cosmogenic [36]Cl concentrations with 1σ uncertainties versus height along Kalafat Fault scarp surface; Blue and orange colors indicate KAL and KALA samples, respectively; (b) Cosmogenic [36]Cl concentrations with 1σ uncertainties versus height along Yavansu Fault scarp surface; G marks the current ground level. (For interpretation of the references to color in this figure legend, the reader is referred to the Web version of this article.)

youngest modeled ruptures (EQ3 to EQ1). The irregular intervals between earthquakes are ca. 4.5 and 1.4 kyr.

6. Discussion

The geochronology of seismic activity of faults can provide essential findings in terms of helping to reduce the potential damages during destructive earthquakes (e.g., Scholz, 2002). The reconstruction of the age and slip amounts of major paleo-earthquakes can make a significant contribution in the field of seismic risk assessment, particularly in the highly populated region of western Anatolia. The activity of several faults prior to the
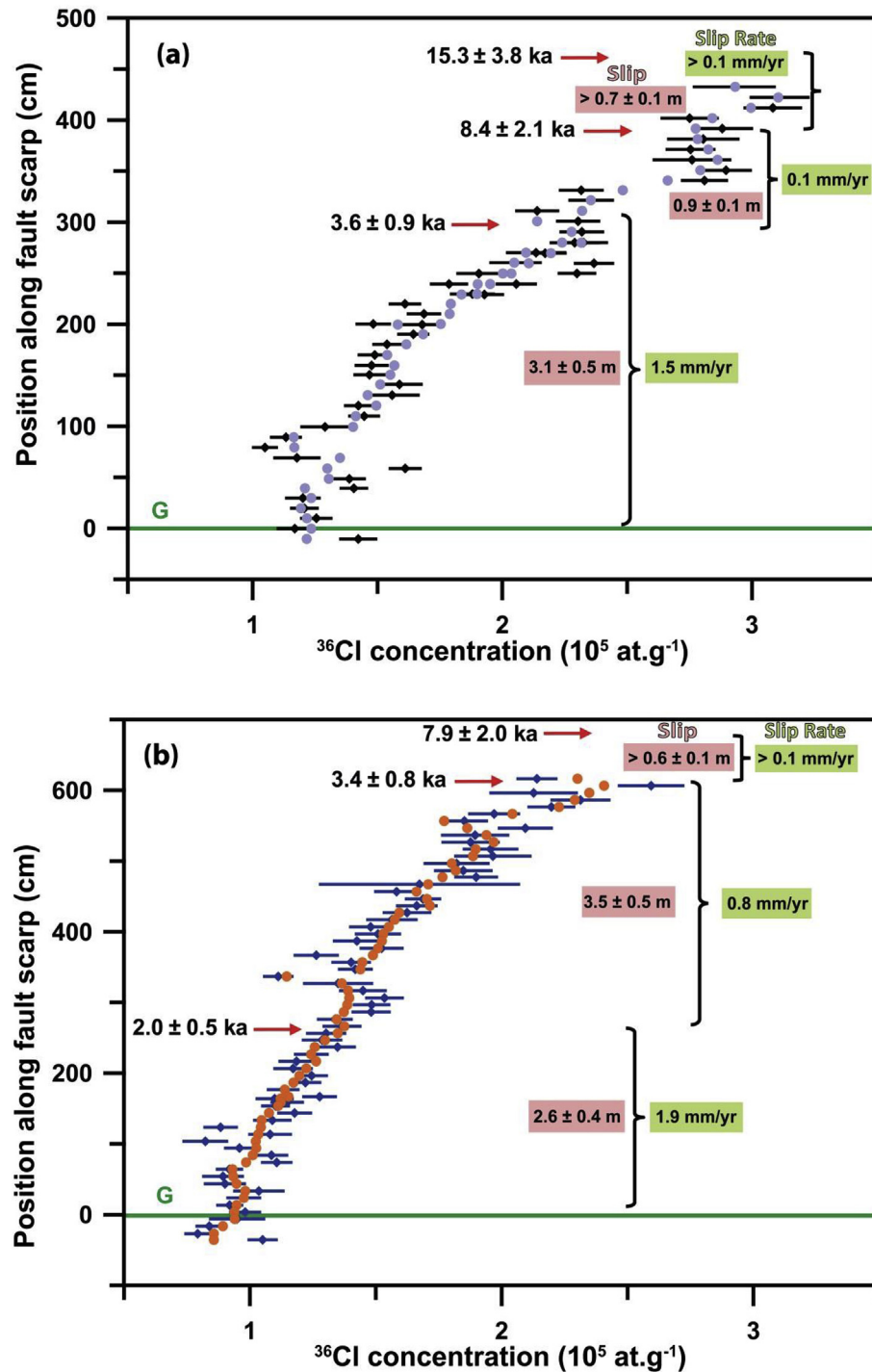
Fig. 6. (a) Best fit (blue circles) of the samples of the Kalafat Fault scarp data with a three rupture model. Black dots with 1σ uncertainties are measured ^{36}Cl concentrations. (b) Best fit (orange circles) of the samples of the Yavansu Fault scarp data with a three rupture model. Blue dots with 1σ uncertainties are measured ^{36}Cl concentrations. Red arrows mark the colluvium positions before the modeled ruptures. Slip rates are calculated individually for each earthquake, based on the slip value and the time period between two successive earthquakes. (For interpretation of the references to color in this figure legend, the reader is referred to the Web version of this article.)

seismic archives in this region has already been documented by the powerful fault scarp dating method on the Priene-Sazlı Fault (Mozafari et al., 2019), as well as the Manastır and Mugırtepe faults in the Manisa Fault Zone (Akçar et al., 2012; Tikhomirov, 2014). This study examined the past seismic activity of the Kalafat and Yavansu faults in western Anatolia using cosmogenic ^{36}Cl. Our results might raise question whether the entire reconstructed slip history is

rather connected to processes of deposition and erosion instead of past earthquake events. We exclude the probability of such large displacements by any other reason, but the successive phases of earthquake activities based on field evidence. In addition, there is no report of remarkable creep along the normal faults in the Aegean area (Pavlides and Caputo, 2004), and this support the idea of normal fault exposure in response to past major earthquakes. In
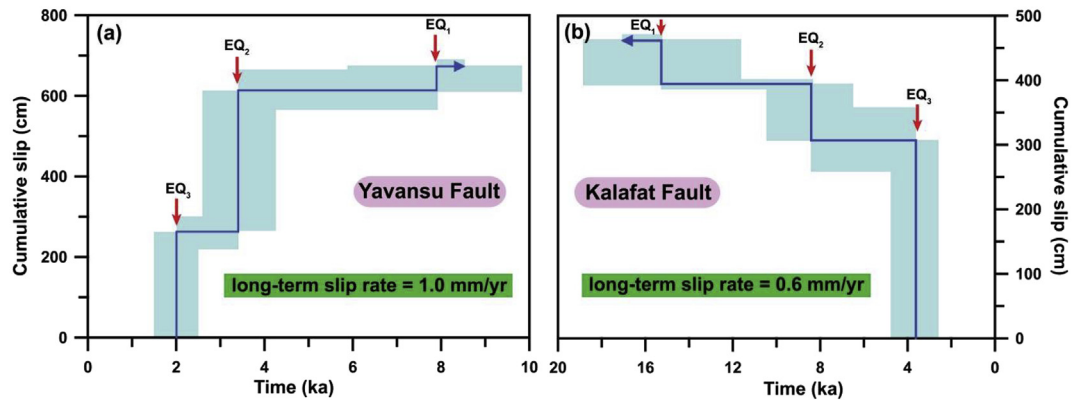
Fig. 7. Time versus cumulative slip amount along with uncertainties of time and colluvium level obtained from modeling of (a) the Yavansu Fault scarp; The average slip rate is 1.0 mm/yr; and (b) the Kalafat Fault scarp; The average slip rate is 0.6 mm/yr.

addition, prevalence of destructive earthquake occurrence in Büyük Menderes graben and its surrounding area documents that the faults activities are responsible for the exposure of fault scarps. Furthermore, many archaeological sites and ancient cities are located in Büyük Menderes graben (e.g., Priene, Miletus and Magnesia), in which the paleo-earthquakes have left evidences of major destructions in the past.

6.1. Earthquake capability

Seismological methods are not yet explicitly able to predict the magnitude of future earthquakes. However, an approximation of probable magnitude is possible based on empirical relationships, which logarithmically connect fault surface length (SRL) to the size of earthquakes. To accomplish this, we used the formula of Pavlides and Caputo (2004), which is specifically based on dip-slip normal faults in the Aegean region (equation (1) in Table 1). The formula of Wells and Coppersmith (1994), which is based on a worldwide investigation on different normal faults, was also used (equation (3) in Table 1). By considering the 15 km length, the Kalafat Fault can produce an earthquake of magnitude 6.5 on average (equation (1) in Table 1). Based on the formula of Wells and Coppersmith (1994) the occurrence of an earthquake with magnitude of 6.4 is possible (equation (3) in Table 1). The probable length of about 10 km for the Yavansu Fault yields an earthquake capacity of magnitude 6.2 or 6.4 in magnitude according to equations (1) and (3), respectively, in Table 1. If the fault is 25 km long, the probable earthquake would have a magnitude of 6.7 and in case of length of 50 km the probable magnitude is estimated to be 7.0 or 7.1 according to equations (1) and (3), respectively, in Table 1, respectively. Since both faults are

able of producing earthquakes of greater than magnitude 5, they can be classified as seismogenic faults (McCalpin, 2009).

The empirical relationships that connect the displacement value with the earthquake magnitude were also used to estimate the possible average slip value as a consequence of probable rupture estimated (i.e., equations (2) and (4) in Table 1). The magnitude of possible earthquakes based on the length of the Kalafat Fault was estimated to be 6.5 (equation (1) in Table 1). This results in a maximum vertical displacement (MVD) and slip of 0.4 m (equation (2) in Table 1). Based on Wells and Coppersmith (1994), the maximum displacement (MD) or slip resulting from an earthquake with magnitude 6.4 is 0.6 m (equation (4) in Table 1). The 10, 25 and 50 km length of the Yavansu Fault yielded earthquakes with magnitudes 6.4, 6.7 and 7.0, respectively (equation (1) in Table 1). The MVD were estimated to be 0.3, 0.7 and 1.4 m, respectively, and based on dip of the fault surface ($\theta = 42°$), yield slips of 0.4, 1.0 and 1.7 m, respectively (equation (2) in Table 1). Considering the formula of Wells and Coppersmith (1994), the maximum displacement (MD) or slip resulting from earthquakes of magnitude 6.2, 6.7 and 7.1 would be 0.4, 0.9 and 2.6 m, respectively (equation (4) in Table 1).

6.2. Earthquake history

In the following paragraphs, we discuss the seismic activity and rupture history of the Kalafat and Yavansu faults based on our modeling, as well as the plausibility of estimated magnitude values of earthquakes that produced the associated amount of slip. We used the same empirical approaches in order to estimate the magnitude values of the reconstructed earthquakes (Pavlides and

Table 1
Regression of SRL (surface rupture length), magnitude (M_s/M) and vertical displacement (MVD/MD) calculated for the Kalafat and Yavansu Faults. Ms (Surface wave magnitude) and M (moment magnitude) value differences are negligible for the earthquakes of larger than 5.7 in Ms (Wells and Coppersmith, 1994). MVD (Maximum Vertical Displacement) is converted to Slip or MD (Maximum Displacement) by applying fault surface dip (Sin (θ) = vertical displacement/Slip).

	SRL/FL	15 km	10 km Duman et al. (2011)	25 km Hancock and Barka (1987)	50 km Hancock and Barka (1987)
Sin (θ) = vertical displacement/slip		KALAFAT FAULT	YAVANSU FAULT		
Pavlides and Caputo (2004)	Ms = 0.9 x Log (SRL) + 5.48 (equation (1))	6.5	6.4	6.7	7.0
	Log (MVD) = 1.14.Ms - 7.82 (equation (2))	MVD = 0.4 Slip = 0.5	MVD = 0.3 Slip = 0.4	MVD = 0.7 Slip = 1.0	MVD = 1.4 Slip = 1.7
Wells and Coppersmith (1994)	M = 4.86 + 1.32 x log (SRL) (equation (3))	6.4	6.2	6.7	7.1
	Log (MD) = - 5.90 + 0.89 x M (equation (4))	MD (Slip) = 0.6	MD (Slip) = 0.4	MD (Slip) = 0.9	MD (Slip) = 2.6

Table 2
Regression of magnitude (M_s/M) and vertical displacement (MVD/MD) for the Kalafat and Yavansu Faults. Unit of slip, MVD and MD is in meters. * Modeled by the code. Ms (Surface wave magnitude) and M (moment magnitude) value differences are negligible for the earthquakes of larger than 5.7 in Ms (Wells and Coppersmith, 1994). MVD (Maximum Vertical Displacement) is converted to Slip or MD (Maximum Displacement) by applying fault surface dip (Sin (θ) = vertical displacement/Slip).

Sin (θ) = vertical displacement/slip		Event	KALAFAT FAULT ($\theta = 84°$)			YAVANSU FAULT ($\theta = 42°$)		
			Slip* (m)	MVD (m)	Ms	Slip* (m)	MVD (m)	Ms
Pavlides and Caputo (2004)	Ms = 0.59 x Log (MVD) + 6.75 (equation (5))		Lowest X^2	Average	Average	Lowest X^2	Average	Average
		EQ1	0.7 ± 0.1	0.7 ± 0.1	6.6	0.6 ± 0.1	0.4 ± 0.1	6.5
		EQ2	0.9 ± 0.1	0.9 ± 0.1	6.8	3.5 ± 0.5	2.3 ± 0.4	7.0
		EQ3	3.1 ± 0.5	3.1 ± 0.5	7.0	2.6 ± 0.4	1.8 ± 0.3	6.9
		Event	KALAFAT FAULT ($\theta = 84°$)		YAVANSU FAULT ($\theta = 42°$)			
			MD (= Slip*) (m)	M	MD (= Slip*) (m)	M		
Wells and Coppersmith (1994)	M = 6.61 + 0.71 x log (MD) (equation (6))		**Lowest X^2**	**Average**	**Lowest X^2**	**Average**		
		EQ1	0.7 ± 0.1	6.5	0.6 ± 0.1	6.5		
		EQ2	0.9 ± 0.1	6.6	3.5 ± 0.5	7.0		
		EQ3	3.1 ± 0.5	7.0	2.6 ± 0.4	6.9		

Caputo, 2004; Wells and Coppersmith, 1994, equations (5) and (6) in Table 2). One should note that EQ1, EQ2 and EQ3 are referred to earthquake events of Kalafat and Yavansu faults, whose plausibility of occurring as either a single or clustered event is discussed below. However EQC1 to EQC4 represent the phases of seismic activity to represent time correlation of earthquake events of both faults.

The locations of our sampling sites on opposite sides of Kalafat Mountain is illustrated in the schematic cross-section shown in Fig. 8a, which shows approximately 120 m of difference in elevation. Based on our modeling, the sampled part of the Kalafat Fault scarp was first exposed at ca. 22 ka. The exact position of the ground level cannot be defined at that time, due to an unsampled part of the scarp. But it was at about 165 m a.s.l. (above sea level) or higher (point G_0 in inset I in Fig. 8b), before the first seismic activity of the Kalafat Fault at 15.3 ± 3.8 ka with a slip value of 0.7 ± 0.1 m (S_1) (EQ1 in inset II in Fig. 8b). This event caused movement of the ground level from G_0 to G_1 (Fig. 6a and inset II in Fig. 8b). For this interval, a slip rate of 0.1 mm/yr was calculated. However, this value is considered as the lower limit, because if the top weathered part was sampled, it might result in a higher slip value. In addition, one should note that we cannot exclude additional older earthquakes, which similarly results in a shorter interval and higher slip rate (e.g., Schlagenhauf et al., 2010). This amount of slip indicates an earthquake with an order of magnitude of 6.5—6.6 (equations (5) and (6) in Table 2). Two earthquakes are required to move the fault to produce this amount of slip (equations (2) and (4) in Table 1). This phase of seismic activity probably occurred as clustered events in a short time span rather than a single earthquake (EQC1 in Fig. 8b). In the South of Kalafat Mountain, the exposure of the sampled fault of the Yavansu Fault appears to be much younger than the Kalafat Fault exposure at ca. 12 ka (inset III in Fig. 8b). Meanwhile the Kalafat Fault ruptured for the second time at 8.4 ± 2.1 ka, after a long phase of inactivity of ca. 6.9 ka. Afterwards, the ground level moved from G_1 to G_2, as a result of 0.9 ± 0.1 m of slip (S_2) (Fig. 6a and inset IV in Fig. 8b). This amount of slip over the time span between the first and second ruptures results in mean slip rate of ca. 0.1 mm/yr. This rupture is likely to be produced by an earthquake of magnitude 6.6 to 6.8 (equations (5) and (6) in Table 2). Two earthquakes are required to expose the fault surface with this amount of slip (equations (2) and (4) in Table 1). The Yavansu Fault started to rupture approximately simultaneously with the second rupture of the Kalafat at 7.9 ± 2.0 ka, with a minimum slip of 0.6 ± 0.1 m (S_1). This caused the initial ground level (G_0) to move to G_1, which was already at the elevation of 43 m a.s.l. or higher before the occurrence of the first rupture (Fig. 6b and insets III and V in Fig. 8b). Similar to the Kalafat Fault, the slip rate of this phase of activity is calculated to be a minimum of 0.1 mm/yr.

This slip amount equals to an MVD of ca. 0.4 m, which can be produced by an earthquake with magnitude of 6.5 (equations (5) and (6) in Table 2). If the 25 or 50 km length of the fault are considered, one earthquake could be severe enough to produce this rupture. However, several earthquakes would be required, if the fault length is 10 km (equations (2) and (4) in Table 1). We consider these two events on the Kalafat and Yavansu faults (EQ2 and EQ1 in insets of IV and V, respectively, in Fig. 8b) as the same phase of activity (EQC2 in Fig. 8b). The last earthquake on the Kalafat Fault occurred at 3.6 ± 0.9 ka after ca. 4.8 kyr period of quiescence. This rupture caused a hanging-wall slip of 3.1 ± 0.5 m (S_3) to the recent ground level of 160 m a.s.l. (Fig. 6a and inset VI in Fig. 8b). The mean slip rate of approximately 1.5 mm/yr was obtained by taking into account the slip amount and the corresponding phase of inactivity from the occurrence of the preceding rupture to the last rupture. An earthquake with magnitude 7 on average is capable of generating this slip (equations (5) and (6) in Table 2). Considering the length of the fault, several earthquakes are required to produce about 3 m of displacement. This phase of activity can also be considered as a series of ruptures that occurred close in time. The second rupture of the Yavansu Fault occurred soon after with the last rupture on the Kalafat Fault at 3.4 ± 0.8 ka, after ca. 4.5 kyr period of quiescence. In total, 3.5 ± 0.5 m of slip (S_2) caused the ground level to move from G_1 to G_2 (Fig. 6b and inset VII in Fig. 8b). The calculated slip rate for this time interval is ca. 0.8 mm/yr, which is much higher than the past phase of activity. The slip amount equates to ca. 2.3 m of MVD, which can be produced by an earthquake of magnitude 7 (equations (5) and (6) in Table 2). More likely, two or more earthquakes were needed to expose the fault with this amount of slip. We conclude that this phase of activity involved a series of ruptures close in time, based on the length of the fault (equations (2) and (4) in Table 1). These two correlated earthquakes (EQ3 and EQ2 in insets of VI and VII, respectively, in Fig. 8b) are also considered as the same phase of activity (EQC3 in Fig. 8b). After a period of quiescence of ca. 1.4 kyr, the last earthquake on the Yavansu Fault occurred at 2.0 ± 0.5 ka ago (EQ3 in insets of VIII in Fig. 8b). This resulted in 2.6 ± 0.4 m of slip (S_3) and the ground level to move to G, the recent ground level of ca. 36 m a.s.l. (Fig. 6b and inset VIII in Fig. 8b). The mean slip rate was about 1.9 mm/yr for this time interval. The slip equals 1.8 ± 0.3 m MVD, which can be created by an earthquake of magnitude 6.9 (equations (5) and (6) in Table 2). One or two earthquakes can cause this slip, where the fault length is considered to be 50 or 25 km long, respectively. If the fault length is 10 km, several earthquakes (EQC4 in Fig. 8b) are responsible for the exposure of the fault in the corresponding period of activity (equations (2) and (4) in Table 1).

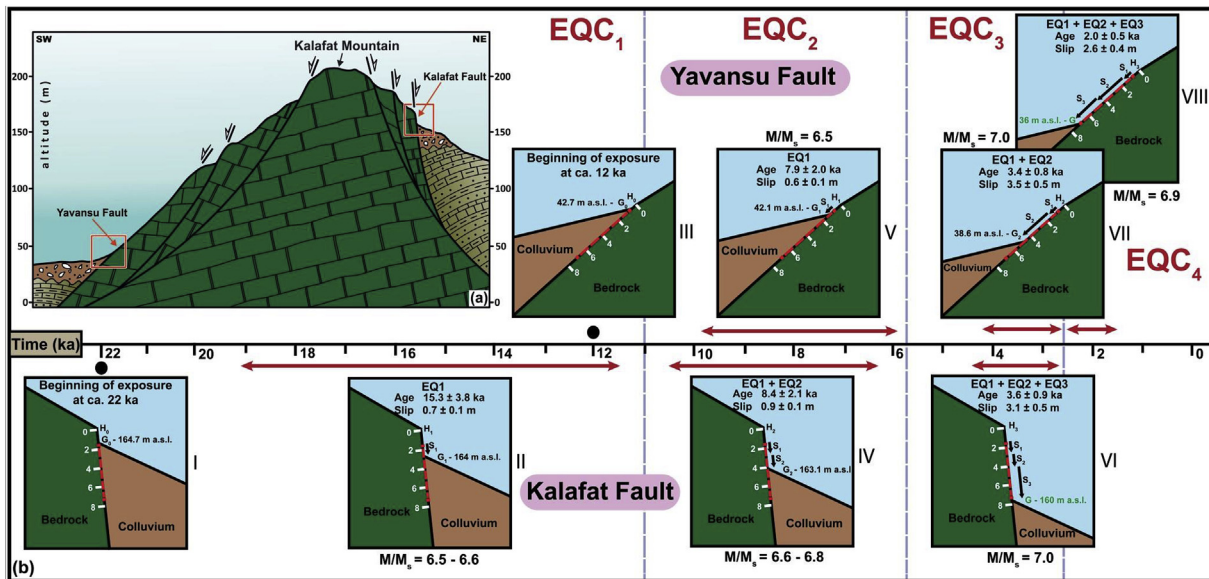The youngest identified earthquake by our modeling dates back

Fig. 8. (a) Schematic sketch of the Yavansu and Kalafat Fault scarps on the opposite sides of the Kalafat Mountain; The horizontal scale is 1:5 (The sampling sites on the Kalafat and Yavansu Fault surfaces are about 1.4 km apart); (b) I to VIII; A detailed view of the fault situation through time, showing colluvium position and episodic fault exposure during three modeled earthquake events (EQ1, EQ2, EQ3), from the beginning of exposure of the Kalafat and Yavansu Faults (left to right). EQC1 to EQC4 are earthquake clusters, representing phases of seismic activity in the area. In the insets, red dashed lines show the sampled surfaces. The fault surface grade is in meters. H_0 shows scarp heights prior to first rupture. H_1 to H_3 are height of the fault scarp following earthquakes of 1–3, respectively; G_0 is ground level just before the first rupture, G_1 and G_2 are ground levels before the second and third ruptures; and G marks the current ground level. S_1 to S_3 represent the associated amounts of slip of three earthquakes from past to recent events. M/M$_s$ show magnitude of earthquake with capacity of displacing the fault with the modeled slip amount. Red double-heading arrows represent the uncertainty of earthquake ages. (For interpretation of the references to color in this figure legend, the reader is referred to the Web version of this article.)

to ca. 2 ka on the Yavansu Fault. However, there are historical and instrumental earthquakes reported, mostly on the Island of Samos since 1751 AD, none of which are directly linked to either the Yavansu or Kalafat faults (Fig. 2). Therefore, our modeling suggests that the western extension of the Yavansu Fault possibly is an individual segment, which is not fully linked to the Yavansu Fault on mainland Turkey. In the Kuşadası region, the cycles of quiescence between successive events along the investigated faults through time are generally shortening. The recurrence interval of earthquakes until the occurrence of the last ruptures of Kalafat and Yavansu faults, are decreasing from ca. 6.9 to 4.8 kyr for the Kalafat Fault and ca. 4.5 to 1.4 kyr for the Yavansu Fault. If we assume the historical and instrumental earthquakes recorded on the Island of Samos (Fig. 2) are related to activity on the Yavansu Fault, and these are not identified by our modeling, an interval of ca. 1.7 kyr is obtained from the last modeled rupture for the Yavansu Fault.

Further south, fault scarp dating of the Priene-Sazlı Fault revealed evidence of four phases of high seismic activity between 8.1 and 2.2 ka with the slip rate increasing from 0.3 to 1.0 mm/yr (Mozafari et al., 2019). Comparison of the timing of the modeled earthquakes on the Kalafat, Yavansu and Priene-Sazlı faults indicates similar timing of high seismic activities in this region at ca. 8 and 3.5 ka, when all three of the faults were active. In addition, at ca. 2 ka, the Priene-Sazlı and Yavansu faults were spontaneously ruptured following a very similar time interval. These data indicate the high amount of dynamic interaction between the nearby faults as a portion of the larger fault setting. Fault interaction plays a key role in development of a fault network in a timescale of a distinct earthquake to millions of years and within distance of tens of kilometres (Nicol et al., 2010). This can cause an increase in fault length and/or cumulative displacement as a consequence of major earthquakes (e.g. Nicol et al., 2010), so that their stress field can trigger earthquakes on nearby faults (Scholz and Gupta, 2000). The probability of propagation of an earthquake from a fault to another

significantly depends on the degree of their interactions (Scholz and Gupta, 2000). It should be noted that triggered earthquakes are differentiated from aftershocks, since aftershocks impacts are restricted only to the mainshock damaged zone. In addition, the magnitude of most significant aftershock basically is at least one unit less than that of mainshock. Based on our results, the Kalafat Fault was exposed ca. 10 kyr prior to the first exposure of the Yavansu Fault, and even had its first significant activity before the Yavansu Fault was exposed (Fig. 8b). This may indicate the possibility of the Yavansu Fault exposure and subsequent activity (EQ2 in inset V, Fig. 8b) triggered by the simultaneous rupture (EQ2 in inset IV, Fig. 8b) and interaction of pre-existing Kalafat Fault as its opposite-facing antithetic pair, which eventually linked through more activities. Evidence for this can be also seen by the increasing slip rates on both faults over time (Figs. 6a, b and 7). Acceleration of slip rates of normal faults can indicate either a cause or an outcome of linkage (e.g., Abruzzo, central Italy; Cowie et al., 2007). In our case study, the increase of the slip rates could cause incremental growth of the Kalafat and Yavansu faults, and ease their linkage. In the Kuşadası Fault Zone, acceleration of slip rates through time together with the existence of relatively short and segmented faults (Fig. 2), which is defined as immaturity (Nicol et al., 2010 and references therein) indicate that the fault system is still propagating and has not reached its final length. This is accordant with our interpretation of the western extension of Yavansu Fault under the sea as a distinct segment, which will subsequently connect to the mainland fault. Shortening of the recurrence interval of earthquakes and increasing slip rates through time could indicate that we can expect the occurrence of major earthquakes in the future with higher frequency. All in all, fault seismic activity and growth are not solely dependent on the local pattern of nearby structures, but are more related to the regional tectonic framework and how the structures are interacted in a large-scale, which might result in either fault lockage or release of accommodated strain.

7. Conclusions

Fault scarp dating using cosmogenic [36]Cl distributions is a powerful technique to recover the history of paleoearthquakes in extensional tectonic settings. In addition, it provides essential information to better understand the fault propagation and linkage history. We have explored the long-term paleoearthquake history of two faults exposed along the western end of the Büyük Menderes Graben prior to and within the available earthquake archives by analyzing cosmogenic [36]Cl in 122 samples and using FSDT (Tikhomirov, 2014). At least six intensive seismic events were recovered, of which two events on each fault happened synchronously. Both faults can be considered as seismic-prone and active faults, which should be given more serious attention in order to reduce the earthquake associated risks. Our findings are summarized as follow:

- Both faults experienced at least three seismic events during late Pleiostocene - Holocene time basically as clusters of earthquakes occurring close in time.
- Vertical components of slips were modeled ranging from 0.7 to 3.1 m for the Kalafat Fault, and from 0.6 to 3.5 m for the Yavansu Fault at the cessation of the seismic events.
- Average slip rates of greater than 0.1, 0.1, and 1.5 mm/yr for the Kalafat Fault and greater than 0.1, 0.8, and 1.9 mm/yr for the Yavansu Fault were estimated from the oldest to youngest modeled ruptures, respectively.
- Long-term slip rates were calculated as 0.6 and 1.0 mm/yr for the Kalafat and Yavansu faults, respectively.
- The recurrence intervals of earthquakes on neither of the faults follow a regular pattern, but are generally getting shorter over time.
- Both Kalafat and Yavansu faults can be considered as seismogenic faults, due to having the potential to generate earthquakes of greater than 6.5 in magnitude.
- At around 3.5 and 8 ka, the three faults of Kalafat, Yavansu and Priene-Sazlı were ruptured as a consequence of major earthquakes, which indicate the occurrence of high seismically active periods in the westernmost part of the Büyük Menderes Graben.
- Most probably the activity of the Yavansu Fault has been triggered by the interaction of the older Kalafat Fault.

Acknowledgments

Appendix A. Supplementary data

Supplementary data to this article can be found online at https://doi.org/10.1016/j.quascirev.2019.07.002.

References

Akçar, N., Tikhomirov, D., Özkaymak, Ç., Ivy-Ochs, S., Alfimov, V., Sözbilir, H., Uzel, B., Schlüchter, Ch., 2012. [36]Cl exposure dating of paleoearthquakes in the eastern Mediterranean: first results from western Anatolian extensional Province, Turkey. GSA Bull. 124 (11/12), 1724—1735.

Alfimov, V., Ivy-Ochs, S., 2009. How well do we understand production of Cl-36 in limestone and dolomite? Quat. Geochronol. 4 (6), 462—474.

Altunel, E., 1998. Evidence for damaging historical earthquakes at Priene, Western Turkey. Turk. J. Earth Sci. 7, 25—35.

Barka, A., Reilinger, R., 1997. Active Tectonics of Eastern Mediterranean region: deduced from GPS, neotectonic and seismicity data. Ann. Geofisc. X2 (3), 587—610.

Beck, J., Wolfers, S., Roberts, J.P., 2018. Bayesian earthquake dating and seismic hazard assessment using chlorine-36 measurements (BED v1). Geosci. Model Dev. 11, 4383—4397.

Benedetti, L., Finkel, R., King, G., Armijo, R., Papanastassiou, D., Ryerson, F.J., Flerit, F., Farber, D., Stavrakakis, G., 2003. Motion on the Kaparelli fault (Greece) prior to the 1981 earthquake sequence determined from Cl-36 cosmogenic dating. Terra. Nova 15 (2), 118—124.

Benedetti, L., Finkel, R., Papanastassiou, D., King, G., Armijo, R., Ryerson, F., Farber, D., Flerit, F., 2002. Post-glacial slip history of the Sparta fault (Greece) determined by Cl-36 cosmogenic dating: evidence for non-periodic earthquakes. Geophys. Res. Lett. 29 (8), 1246. https://doi.org/10.1029/2001GL014510.

Benedetti, L., Manighetti, I., Gaudemer, Y., Finkel, R., Malavieille, Y., Pou, Kh., Arnold, M., Aumaître, G., Bourlès, D., Keddadouche, K., 2013. Earthquake synchrony and clustering on Fucino faults (Central Italy) as revealed from in situ [36]Cl exposure dating. J. Geophys. Res. Solid Earth 118, 4948—4974.

Carcaillet, J., Manighetti, I., Chauvel, C., Schlagenhauf, A., Nicole, J.M., 2008. Identifying past earthquakes on an active normal fault (Magnola, Italy) from the chemical analysis of its exhumed carbonate fault plane. Earth Planet. Sci. Lett. 271, 145—158.

Christl, M., Vockenhuber, C., Kubik, P.W., Wacker, L., Lachner, J., Alfimov, V., Synal, H.A., 2013. The ETH Zurich AMS facilities: performance parameters and reference materials. Nucl. Instrum. Methods Phys. Res. B 294, 29—38.

Cowie, P.A., Phillips, R.J., Roberts, G.P., McCaffrey, K., Zijerveld, L.J.J., Gregory, L.C., Faure Walker, J., Wedmore, L.N.J., Dunai, T.J., Binnie, S.A., Freeman, S.P.H.T., Wilcken, K., Shanks, R.P., Huismans, R.S., Papanikolaou, I., Michetti, A.M., Wilkinson, M., 2017. Orogen-scale uplift in the central Italian Apennines drives episodic behaviour of earthquake faults. Sci. Rep. 7. Article number 44858.

Cowie, P.A., Roberts, G.P., Mortimer, E., 2007. Strain localization within fault arrays over timescales of 10^0-10^7 years (Observations, explanations, and debates) In: Handy, M.R., Hirth, G., Hovius, N. (Eds.), Tectonic Faults: Agents of Change on a Dynamic Earth. MIT Press, Cambridge, Mass, pp. 47—78.

Dewey, J.F., Şengör, A.M.C., 1979. Aegean and surrounding region: complex multi-plate and continuum tectonics in a convergent zone. Geol. Soc. Am. Bull. 90, 84—92.

Duman, T.Y., Emre, Ö., Özalp, S., Elması, H., 2011. Active Fault Map Series of Turkey (Scale 1:250,000), General Direct. Mineral Res. Explor., Aydın (NJ 35-11).

Elmore, D., Ma, X., Miller, T., Mueller, K., Perry, M., Rickey, F., Sharma, P., Simms, P., Lipschutz, M., Vogt, S., 1997. Status and plans for the PRIME Lab AMS facility. Nucl. Instrum. Methods Phys. Res. Sect. B Beam Interact. Mater. Atoms 123 (1—4), 69—72.

Emre, Ö., Duman, T.Y., Özalp, S., Şaroğlu, F., Olgun, Ş., Elması, H., Tolga, Ç., 2016. Active fault database of Turkey. Bull. Earthq. Eng. https://doi.org/10.1007/s10518-016-0041-2.

Evans, J.M., Stone, J.O.H., Fifield, L.K., Cresswell, R.G., 1997. Cosmogenic chlorine-36 production in K-feldspar. Nucl. Instrum. Methods Phys. Res. Sect. B Beam Interact. Mater. Atoms 123 (1—4), 334—340.

Fink, D., Vogt, S., Hotchkis, M., 2000. Cross-sections for Cl-36 from Ti at E-p=35-150 MeV: applications to in-situ exposure dating. Nucl. Instrum. Methods Phys. Res. Sect. B Beam Interact. Mater. Atoms 172, 861—866.

Gürer, Ö.F., Sarica-Fileoreau, N., Özburan, M., Sangu, E., Doğan, B., 2009. Progressive development of the Büyük Menderes Graben based on new data, western Turkey. Geol. Mag. 146 (5), 652—673.

Hancock, P.L., Barka, A.A., 1987. Kinematic indicators on active faults in western Turkey. J. Struct. Geol. 9 (5/6), 573—584.

Ivy-Ochs, S., Poschinger, A.V., Synal, H.A., Maisch, M., 2009. Surface exposure dating of the Flims landslide, Graubunden, Switzerland. Geomorphology 103 (1), 104—112.

Ivy-Ochs, S., Synal, H.A., Roth, C., Schaller, M., 2004. Initial results from isotope dilution for Cl and Cl-36 measurements at the PSI/ETH Zurich AMS facility. Nucl. Instrum. Methods Phys. Res. Sect. B Beam Interact. Mater. Atoms 223—24, 623—627.

Koçyiğit, A., Özaçar, A.A., 2003. Extensional neotectonic regime through the NE edge of the Outer Isparta Angle, SW Turkey: new field and seismic data. Turk. J. Earth Sci. 12, 67—90.

Liu, B.L., Phillips, F.M., Fabrykamartin, J.T., Fowler, M.M., Stone, W.D., 1994. Cosmogenic [36]Cl accumulation in unstable landforms, 1. Effects Therm. Neutron Distrib.: Water Resour. Res. 30 (11), 3115—3125.

McCalpin, J.P. (Ed.), 2009. Paleoseismology. Academic, London, p. 629.

Mechernich, S., Schneiderwind, S., Mason, J., Papanikolaou, I., Deligiannakis, G., Pallikarakis, A., Binnie, S.A., Dunai, T.J., Reicherter, K., 2018. The seismic history of the Pisia fault (eastern Corinth rift, Greece) from fault plane weathering features and cosmogenic [36]Cl dating. J. Geophys. Res. Solid Earth 123 (5), 4266—4284.

Mitchell, S.G., Matmon, A., Bierman, P.R., Enzel, Y., Caffee, M., Rizzo, D., 2001. Displacement history of a limtesone normal fault scarp, northern Israel, from

cosmogenic ^{36}Cl. J. Geophys. Res. 106 (B3), 4247–4264.

Mouslopoulou, V., Moraetis, D., Benedetti, L., Guillou, V., Bellier, O., Hristopulos, D., 2014. Normal faulting in the forearc of the Hellenic subduction margin: paleoearthquake history and kinematics of the Spili Fault, Crete, Greece. J. Struct. Geol. 66, 298–308.

Mozafari, N., Sümer, Ö., Tikhomirov, D., Ivy-Ochs, S., Alfimov, V., Vockenhuber, Ch., İnci, U., Sözbilir, H., Akçar, N., 2019. Holocene seismic activity of the Priene-Sazlı Fault revealed by cosmogenic ^{36}Cl, western Anatolia, Turkey. Turk. J. Earth Sci. 28, 410–437. https://doi.org/10.3906/yer-1810-6.

Nicol, A., Walsh, J.J., Villamor, P., Seebeck, H., Berryman, K.R., 2010. Normal fault interactions, paleoearthquakes and growth in an active rift. J. Struct. Geol. 32, 1101–1113.

Palumbo, L., Benedetti, L., Bourles, D., Cinque, A., Finkel, R., 2004. Slip history of the Magnola fault (Apennines, Central Italy) from ^{36}Cl surface exposure dating: evidence for strong earthquake over the Holocene: earth planet. Sci. Lett. 225, 163–176.

Pavlides, S., Caputo, R., 2004. Magnitude versus faults' surface parameters: quantitative relationships from the Aegean Region. Tectonophysics 380, 159–188.

Phillips, F.M., Stone, W.D., Fabryka-Martin, J.T., 2001. An improved approach to calculating low-energy cosmic-ray neutron fluxes near the land/atmosphere interface. Chem. Geol. 175 (3–4), 689–701.

Phillips, F.M., Zreda, M.G., Flinsch, M.R., Elmore, D., Sharma, P., 1996. A reevaluation of cosmogenic Cl-36 production rates in terrestrial rocks. Geophys. Res. Lett. 23 (9), 949–952.

Schimmelpfennig, I., Benedetti, L., Finkel, R., Pik, R., Blard, P.H., Bourles, D., Burnard, P., Williams, A., 2009. Sources of in-situ Cl-36 in basaltic rocks. Implications for calibration of production rates. Quat. Geochronol. 4 (6), 441–461.

Schlagenhauf, A., Gaudemer, Y., Benedetti, L., Manighetti, I., Palumbo, L., Schimmelpfennig, I., Finkel, R., Pou, K., 2010. Using in situ chlorine-36 cosmonuclide to recover past earthquake histories on limestone normal fault scarps: a reappraisal of methodology and interpretations. Geophys. J. Int. 182 (1), 36–72.

Schlagenhauf, A., Manighetti, I., Benedetti, L., Gaudemer, Y., Finkel, R., Malavieille, J., Pou, K., 2011. Earthquake supercycles in Central Italy, inferred from ^{36}Cl exposure dating. Earth Planet. Sci. Lett. 307 (3–4), 487–500.

Scholz, Ch. H., 2002. The Mechanics of Earthquakes and Faulting, second ed. Cambridge University Press, p. 464.

Scholz, C.H., Gupta, A., 2000. Fault interactions and seismic hazard. J. Geodyn. 29, 459–467.

Soysal, H., Sipahioğlu, S., Kolçak, D., Altınok, Y., 1981. Historical Earthquake Catalogue of Turkey and Surrounding Area (2100 B.C.-1900 A.D.). Technical Report. TUBİTAK. No: TBAG-341.

Stone, J.O., 2000. Air pressure and cosmogenic isotope production. J. Geophys. Res. 105 (B10), 23753–23759.

Stone, J.O., 2005. Terrestrial chlorine-36 production from spallation of iron. In: 10th International Conference on Accelerator Mass Spectrometry. Berkeley, California.

Stone, J.O., Allan, G.L., Fifield, L.K., Cresswell, R.G., 1996. Cosmogenic chlorine-36 from calcium spallation. Geochem. Cosmochim. Acta 60, 679–692.

Stone, J.O., Evans, J.M., Fifield, L.K., Allan, G.L., Cresswell, R.G., 1998. Cosmogenic chlorine-36 production in calcite by muons. Geochem. Cosmochim. Acta 62 (3), 433–454.

Sümer, Ö., Inci, U., Sözbilir, H., 2012. Tectono-sedimentary evolution of an Early Pleistocene shallow marine fan-deltaic succession at the western coast of Turkey. Geodin. Acta 25 (Nos. 3–4), 112–131.

Sümer, Ö., İnci, U., Sözbilir, H., 2013. Tectonic evolution of the Söke basin: extension-dominated transtensional basin formation in western part of the Büyük Menderes graben, western Anatolia, Turkey. J. Geodyn. 65, 148–175.

Synal, H.A., Bonani, G., Dobeli, M., Ender, R.M., Gartenmann, P., Kubik, P.W., Schnabel, C., Suter, M., 1997. Status report of the PSI/ETH AMS facility. Nucl. Instrum. Methods Phys. Res. Sect. B Beam Interact. Mater. Atoms 123 (1–4), 62–68.

Tesson, J., Pace, B., Benedetti, L., Visini, F., Delli Rocioli, M., Arnold, M., Aumaître, G., Bourlès, D.L., Keddadouche, K., 2016. Seismic slip history of the Pizzalto fault (central Apennines, Italy) using in situ-produced 36Cl cosmic ray exposure dating and rare earth element concentrations. J. Geophys. Res. Solid Earth 121, 1983–2003.

Tesson, J., Benedetti, L., 2019. Seismic history from in situ 36Cl cosmogenic nuclide data on limestone fault scarps using Bayesian reversible jump Markov chain Monte Carlo. Quat. Geochronol. 52, 1–20.

Tikhomirov, D., 2014. An Advanced Model for Fault Scarp Dating and Paleoearthquake Reconstruction, with a Case Study of the Gediz Graben Formation (Turkey). PhD thesis. University of Bern.

Tikhomirov, D., Akcar, N., Ivy-Ochs, S., Alfimov, V., Schlüchter, C., 2014. Calculation of shielding factors for production of cosmogenic nuclides in fault scarpes. Quat. Geochronol. 19, 181–193.

Wells, D.L., Coppersmith, J.K., 1994. New empirical relationships among magnitude, rupture length, rupture width, rupture area, and surface displacement. Bull. Seismol. Soc. Am. 84, 974–1002.

Zreda, M., Noller, J., 1998. Ages of prehistoric earthquakes revealed by cosmogenic chlorine-36 in a bedrock fault scarp at Hebgen Lake. Science 282, 1097–1099.

Zreda, M.G., Phillips, F.M., Elmore, D., Kubik, P.W., Sharma, P., Dorn, R.I., 1991. Cosmogenic chlorine-36 production rates in terrestrial rocks. Earth Planet. Sci. Lett. 105, 94–109.